www.sciencemag.org/content/353/6301/794/suppl/DC1

Supplementary Materials for

Quantum thermalization through entanglement in an isolated many-body system

Adam M. Kaufman, M. Eric Tai, Alexander Lukin, Matthew Rispoli, Robert Schittko, Philipp M. Preiss, Markus Greiner*

*Corresponding author. Email: greiner@physics.harvard.edu

Published 19 August 2016, *Science* **353**,794 (2016)
DOI: 10.1126/science.aaf6725

This PDF file includes:

1 Eigenstate Thermalization Hypothesis

Here we provide a brief summary of the Eigenstate Thermalization Hypothesis (ETH) and its relationship to our experiment. Generically, a quenched quantum state consists of a superposition of many-body energy eigenstates, each of which evolves according to the frequency of the associated eigenenergy E_n. For the state $|\psi(t)\rangle = \sum_n c_n e^{-iE_n t} |n\rangle$, the observable $\langle \mathcal{O}(t) \rangle$ evolves according to,

$$\langle \mathcal{O}(t) \rangle = \sum_{\alpha,\beta} c_\alpha^* c_\beta e^{i(E_\alpha - E_\beta)t/\hbar} \mathcal{O}_{\alpha\beta}$$

$$\langle \mathcal{O}(t) \rangle = \underbrace{\sum_{\alpha} |c_\alpha|^2 \mathcal{O}_{\alpha\alpha}}_{\mathcal{S}_{\text{diag}}} + \underbrace{\sum_{\alpha,\beta\neq\alpha} c_\alpha^* c_\beta e^{i(E_\alpha - E_\beta)t/\hbar} \mathcal{O}_{\alpha\beta}}_{\mathcal{S}_{\text{off}}}$$

where $\mathcal{O}_{\alpha\beta} = \langle \alpha | \mathcal{O} | \beta \rangle$ for the energy eigenstates $|\alpha\rangle$ and $|\beta\rangle$. We consider the system to thermalize if

1. the first term, $\mathcal{S}_{\text{diag}}$, takes a value $\overline{\mathcal{O}}$ that matches the microcanonical prediction
2. the second term, $\mathcal{S}_{\text{off}}$, has only small fluctuations around zero for long times

Regarding condition 1, the microcanonical ensemble predicts a value for macroscopic observables that depends only on the average energy of the system. However, $\mathcal{S}_{\text{diag}}$ explicitly contains terms related to the initial population distribution, which suggests the saturated value of the observable depends on initial details of the system, rather than just the average energy. ETH resolves this puzzle by stating that a quantum quench populates mostly the eigenstates far from the edge of the spectrum, and that these eigenstates approximate those of random matrix theory. ETH proposes that these eigenstates look locally thermal and the expectation value of local observables varies smoothly between eigenstates close in energy. This implies that the exact probabilities from condition $\mathcal{S}_{\text{diag}}$ are not quantitatively relevant in the sum, since the $\mathcal{O}_{\alpha,\alpha}$ can be approximately factored out. Regarding condition 2, while for times short compared to the spread in populated eigenfrequencies the relative phases of each component in $\mathcal{S}_{\text{off}}$ are fine-tuned to match the initial state, at long times the relative phases are randomized. Ostensibly, this dephasing ensures that $\mathcal{S}_{\text{off}} \to 0$, but the time scale for this process is given by the "typical" value of the smallest gap in the spectrum. In a general many-body system, this value can be exponentially small which would lead to an infinite thermalization time, but for the systems where ETH applies level repulsion ensures that this "typical" gap value stays finite (13). As important, ETH states that the off-diagonals of $\mathcal{O}$ in the eigenbasis are negligible compared to the on-diagonals, so that this second term damps to a value which does not influence the steady-state of $\langle \mathcal{O} \rangle$. For a more detailed summary of ETH, we point the reader to Refs. (7, 13).

2 Computing expectation values in thermalized systems

ETH implies an equivalence between the local expectation values of a quenched many-body state and those of the thermal density matrix with the same average total energy as the many-body state. For the reported experiments, our system is initialized into the ground state, $|\psi_0\rangle$, of an initial Hamiltonian, $\mathcal{H}_0$, in the atomic limit. At $t = 0$, we quench the system into a Hamiltonian, $\mathcal{H}_q$, after which the system is allowed to evolve for a variable amount of time. Comparing to the data at longs times ($10 - 20$ ms, where we observe saturation), we can compute predictions for the expectation values of various local observables based upon different thermodynamic ensembles. These predictions are computed using the following procedures.

Microcanonical Ensemble

The microcanonical ensemble is an equal probability statistical mixture of all the eigenstates that lie within an energy interval given by the initial state $|\psi_0\rangle$. In the quenched Hamiltonian, the initial state has an energy

$$E^{(0)} \equiv \langle \psi_0 | \mathcal{H}_q | \psi_0 \rangle$$

while the eigenstates of $\mathcal{H}_q$, $\left|\phi_i^{(q)}\right\rangle$, have energies $E_i^{(q)}$. The microcanonical ensemble is then composed of the N_{MC} number of eigenstates for which $|E_i^{(q)} - E^{(0)}| < \delta E$. For our numerical data, we have chosen $\delta E = 0.2J$, but the ensemble predictions are insensitive to the precise value of δE. The microcanonical ensemble can be represented by the thermal density matrix

$$\rho_{ij}^{MC} = \begin{cases} \frac{1}{N_{\mathrm{MC}}}, & \text{if } i = j \text{ and } |E_i^{(q)} - E^{(0)}| < \delta E \\ 0, & \text{else} \end{cases}.$$

Canonical Ensemble

The canonical ensemble is a statistical mixture of all the eigenstates in the system weighted by each state's Boltzmann factor, $\exp(-E_i^{(q)}/k_B T)$. The temperature in the Boltzmann factor is fixed through the stipulation that the average energy of this thermal ensemble matches the energy of the initial state, i.e. we choose T such that

$$\mathrm{Tr}(\mathcal{H}_q \rho^{CE}) = \langle\psi_0| \mathcal{H}_q |\psi_0\rangle ,$$

where the thermal density matrix ρ^{CE} has the following construction,

$$\rho_{ij}^{CE} = \begin{cases} e^{-\frac{E_i^{(q)}}{k_B T}}, & \text{if } i = j \\ 0, & \text{else} \end{cases}.$$

Single Eigenstate Ensemble

Energy eigenstates of systems conforming to ETH are surmised to appear thermal in local observables. We numerically calculate the eigenstates of the quenched Hamiltonian and compare the experimentally observed local counting statistics to the prediction from the single full system eigenstate $\left|\phi_i^{(q)}\right\rangle$ that is closest in energy to the expectation value $E^{(0)}$. The expectation value in this case is given by,

$$\langle\mathcal{A}\rangle_{\mathrm{SE}} = \left\langle\phi_i^{(q)}\right| \mathcal{A} \left|\phi_i^{(q)}\right\rangle .$$

Diagonal Ensemble

The diagonal ensemble is a statistical mixture of all eigenstates of the full Hamiltonian $\mathcal{H}_q$, with the weights given by their amplitudes after quench.

$$\rho_{ij}^{D} = \begin{cases} |\left\langle\psi_0\right|\left.\phi_i^{(q)}\right\rangle|^2, & \text{if } i = j. \\ 0, & \text{else} \end{cases}$$

It carries all information about the amplitudes of the eigenstates but ignores all their relative phases.

Grand Canonical Ensemble

The grand-canonical ensemble requires calculating the temperature and chemical potential for the subsystem associated to the observable of interest. For example, the top (bottom) row of FIG. 6C pertains to the subsystem consisting of the third site (the first three sites) of the chain. We calculate the temperature and chemical potential for the subsystem as follows. Because the energy and particle number within the subsystem are not conserved during the quench dynamics, we must compute the average energy $\langle E_A\rangle$ and average number $\langle N_A\rangle$ within the subsystem numerically. We time-evolve the full many-body state to the thermalized regime, then compute the reduced density matrix for the subsystem, with which we can calculate $\langle N_A\rangle$ and $\langle E_A\rangle$. We note that the average energy of nearly all the subsystems is very close to that of the full system (zero), while the average number is nearly consistent with unity particle density. For the single site subsystems, however, there is no tunneling term to offset the interaction energy, and therefore these subsystems have non-zero energy. We perform this full calculation to account for finite-size effects that cause

small temporal energy and number fluctuations. If we neglect the energy fluctuations, the grand-canonical predictions (described below) are negligibly different.

After the above calculations, we can compute the chemical potential and temperature. Using each H_A^N, the subsystem Bose-Hubbard Hamiltonian with N particles, we compute the eigenstates ($|E_A^{N,i}\rangle$, where i indexes the eigenstate) and energies ($E_A^{N,i}$) for each particle sector. We seek T and μ such that,

$$\langle N_A \rangle = \langle N_{\mathrm{GCE}} \rangle = \frac{1}{Z} \sum_{i,N} N e^{-(E_A^{N,i} - \mu N)/k_B T}$$

and,

$$\langle E_A \rangle = \langle E_{\mathrm{GCE}} \rangle = \frac{1}{Z} \sum_{i,N} E_A^{N,i} e^{-(E_A^{N,i} - \mu N)/k_B T},$$

where for each particle number N, the index i is summed over all eigenstates within that number sector. The partition function, Z, is the overall normalization. These equations are numerically solved to find μ and T. With these in hand, we arrive at the grand-canonical ensemble,

$$\rho_{\mathrm{GCE}} = \frac{1}{Z} \sum_{i,N} |E_A^{N,i}\rangle\langle E_A^{N,i}| e^{-(E_A^{N,i} - \mu N)/k_B T}.$$

Observables

For all statistical ensembles above, expectation values of an observable $\mathcal{A}$ are calculated from the density matrix as

$$\langle \mathcal{A} \rangle = \mathrm{Tr}(\mathcal{A}\rho),$$

where ρ is the full system density matrix corresponding to the appropriate ensemble.

3 Entropies

3.1 Rényi Entropy

All entanglement entropy values discussed in the main text are defined as a function of the reduced density matrix of the subsystem. This applies also for the thermal entropies quoted in the main text, where we use the reduced density matrix of the canonical ensemble described above. The entropy metric used for comparison between the quantum system we measure and the canonical thermal ensemble is the Rényi entropy. In general, the n-th order Rényi entropy is defined for a reduced density matrix of subsystem A as

$$S_n(\rho_A) = \frac{1}{1-n} \log\left(\mathrm{Tr}[\rho_A^n]\right),$$

where the reduced density matrix ρ_A is defined by tracing out all degrees of freedom of the system that do not include subsystem A

$$\rho_A = \mathrm{Tr}_B(\rho_{AB}).$$

Experimentally, we interfere two identical quantum states to obtain simultaneously the global and local purity ($\mathrm{Tr}(\rho_A^2)$). Therefore the relevant order Rényi entropy is the second-order ($n = 2$) Rényi entropy which is defined for a density matrix of subsystem as

$$S_2(\rho_A) = -\log\left(\mathrm{Tr}[\rho_A^2]\right),$$

and is also important qualitatively as a lower bound of the von Neumann entropy. When discussing the global purity as an entropy, we use the Rényi formulation in terms of the global density matrix ρ as opposed to a reduced density matrix ρ_A. Lastly, note that we use logarithms to base e throughout.

It is important to stress that the thermodynamic relations defined from statistical mechanics with the von Neumann definition do not directly apply for the Rényi definition. However, both quantities measure the incoherent diffusion in Hilbert space associated with entropy, and the Rényi entropy is directly accessible by our measurements.

3.2 Simulations

All simulations use measured experimental parameters from Table S1 to construct the Hamiltonian. The shown theory curves are computed through direct diagonalization of the Hamiltonian given the relevant Bose-Hubbard parameters. The inital state is the exact Mott insulating ground state of both lattices at $45E_r$. The 1-D quench dynamics are then simulated by projecting this initial state onto the eigenstates of the quenched Bose-Hubbard Hamiltonian and evolved in time by their corresponding eigenvalues. The full density matrix can then be constructed at any time t and traced for either the on-site number statistics or entanglement entropy to be compared with the data. The plotted theory have zero-fit parameters, and are only corrected for overall offsets due to the measured residual extensive entropy in the data (see Section 4). We also include a temporal offset of 0.5 ms that is the same for all theory calculations, which is based on an independent numerical model of the (nearly perfectly diabatic) ramp that realizes the quench. Besides this offset, we have confirmed numerically that the degree to which this ramp is not perfectly diabatic does not influence the results.

4 Experimental Sequence

State Preparation

Our experiments start with a unity filling, two-dimensional Mott insulator of ^{87}Rb atoms in a deep lattice ($V_x = V_y = 45E_r$) with 680 nm spacing. We utilize a DMD in the Fourier plane to initialize a plaquette of 2×6 atoms using a procedure outlined in previous work (24). We achieve a single site plaquette loading fidelity of $\sim 93\%$, which is limited by the fidelity of the initial Mott insulator and losses during the preparation sequence.

To study the dynamics in the quenched system, we project an optical potential consisting of two narrow Gaussian peaks separated by 6 lattice sites in the x-direction and a flat-top profile in the y-direction. This confinement provides the atoms with a "box"-like potential superimposed upon and registered to the lattice position. By changing V_x from $45E_r$ to $6E_r$ in 0.75 ms (70 ms) while retaining $V_y = 45E_r$ we realize identical diabatic (adiabatic) evolution in 1-D 6-site chains. After some evolution time we rapidly freeze the dynamics by ramping the lattice along x-direction to $20E_r$. We can then conduct two types of experiments on the final state of the system: perform a single site resolved atom number counting or measuring the entropy of the state by means of a beam splitter operation.

Single-site resolved atom number counting

In this section, we outline our procedure for counting the total atom number on each site of the 2x6 plaquette. After freezing the atom dynamics, we project a narrow (along the y-direction) Gaussian potential. We then drop $V_y = 0E_r$ while keeping $V_x = 45E_r$, separating the atoms away from the partition while preserving their position in the x-direction. After 2 ms of free evolution in the half tubes we pin the atom positions with the imaging lattice ($3000E_r$) and perform fluorescence imaging of the atoms. The total population of each half tube corresponds to the original population of a particular lattice site in each of the two copies. During the expansion process atoms delocalize uniformly over $\sim$50 lattice sites. The majority of our outcomes ($\sim 96\%$) contain 3 or fewer particles per site which results in probability of particle loss due to parity projection $< 6\%$. We do not apply a correction for this effect because it is smaller than the statistical error for the majority of data points.

Entanglement entropy

We measure global purity and entanglement entropy by applying an atomic beam splitter and interfering the two copies of the 6-site system. We perform the beam splitter operation by projecting a double-well potential along y that is superimposed on the lattice. The tunnel-coupling of the double-well is set by a combination of both the y lattice and this projected potential, which is nearly uniform along the x direction. After diabatically reducing $V_y = 2E_r$, the atoms tunnel in the double-wells for 0.33 ms, which corresponds to the single particle balanced beam splitter time (24). This operation results in a two-particle oscillation

contrast of $\sim 96\%$. We infer the purity of any given subsystem by computing the average parity given by $\mathrm{Tr}(\rho_A^2) = \langle P^i \rangle = \langle \prod_{k \in A} p_k^i \rangle$, where $i = 1, 2$ denotes one of the output modes of the double-well and $p_k^i = \pm 1$ denotes the parity of a given mode (4).

Extensive background entropy

The imperfect fidelity of the beam splitter operation reduces the interference contrast between the two many-body systems. The measured purities hence underestimate the purity of the many-body states produced in the experiment.

We verify experimentally that this entropy background contributed by imperfections is extensive. For a separable many-body state, such as a Mott insulator in the atomic limit, we observe an entropy of 0.34 for the full system, or 0.06 per site.

For the relevant case of superfluid ground states and highly excited quenched states, the measured full system entropy is increased to 0.63. We attribute this increase in measured entropy to the sensitivity of such states to differences in the Hamiltonian between the two copies: During the short 3 ms hold time between the state preparation and the beam splitter operation, potential differences on the 5 Hz level can lead to a differential dephasing between the two copies and a reduced interference contrast. We therefore minimize the hold time and use an intermediate lattice depth ($20E_r$).

We confirm the additive, extensive nature of this background entropy by subtracting the theoretical predicted value of entropy from the measured one as a function of the system size, which shows linear growth of this quantity within our statistics (see Fig. S2). By fitting the data we extract the slope of the curve and apply the correction given by the subsystem size to different plots (see Table S2). With the exception of very short times, these data affirm that the extensive corrections are substantially smaller than the entanglement entropy we measure.

Bose-Hubbard parameters

Experimental parameters for the state preparation and quenches to different temperatures are shown in Table S1. The temperatures tabulated correspond to the canonical ensemble, as described in Section 2. We calibrate lattice depths through modulation spectroscopy in a deep $45E_r$ lattice with a typical uncertainty of $\pm 2\%$ and obtain J from a band structure calculation. U is measured through photon-assisted tunneling at a lattice depth of $V_x = 16E_r$ and numerically extrapolated to lower depths, taking into account corrections due to higher bands. Throughout the manuscript, the measured entanglement entropy and counting statistics are compared to numerical solutions of the Schrödinger equation with the appropriate Bose-Hubbard parameters.

5 Data analysis

Post-selection

Before analyzing the data, we post-select on the outcomes containing 6 particles in each copy for the site-resolved number detection (FIG. 5,6). We post-select on total of 12 atoms for in both copies for experiments in which we perform the beam splitter operation. Outcomes containing lower particle number are attributed to the instances of imperfect plaquette loading or atom loss during the experimental sequence. We thus retain approximately 30% of the original data.

Data averaging

For all entanglement entropy data we average over both copies after the beam splitter operation. Additionally, we take the mean of equivalent symmetric subsystems in each copy for entanglement entropy dynamics (FIG. 3), for the volume law data (FIG. 4A) we average over all contiguous subsystems of the given size. Finally, for the data in FIG. 4B,C, we average over all contiguous and non-contiguous subsystems of the given volume, because the mutual information can sample correlations between non-contiguous subsystems. For all of the entanglement entropy data, the error bars are S.E.M. For all of the number counting, the error

bars are S.E.M. except when stated otherwise. For the entanglement entropy and number counting data, typically 100-200 post-selected runs of the experiment are used to create each data point in the plots.

Quantifying the early time time dynamics of the entanglement entropy

In an inset of FIG. 3, we quantify the growth of entanglement entropy in the early time dynamics. We approximate this growth as linear, while the long time dynamics as flat. We fit the data with a piecewise function,

$$S_2(t) = \begin{cases} S_g \cdot t, & \text{if } t \leq t_{\text{sat.}} \\ S_g \cdot t_{\text{sat.}}, & \text{else} \end{cases},$$

where the slope S_g and saturation time $t_{\text{sat.}}$ are left as free parameters (Fig. S3). The fitted value of S_g is quoted in the text for the slope.

Figures and Tables

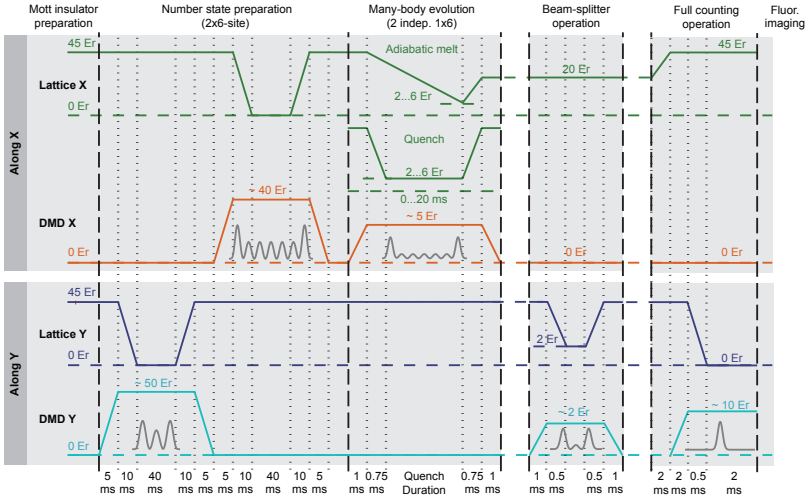

Figure S1: Schematic showing the ramps of the lattices and DMD potentials in the x- and y-directions during the experimental sequence. The projected DMD potentials are drawn in the labeled direction where the orthogonal direction of the potential is a smooth, flat-top profile. The break for the beam splitter operation is shown as an optional step taken during the sequence. Performing this operation results in the sequence measuring the local and global system purity while not performing this step results in the sequence measuring the on-site number statistics. All ramps are exponential in depth as a function of time.

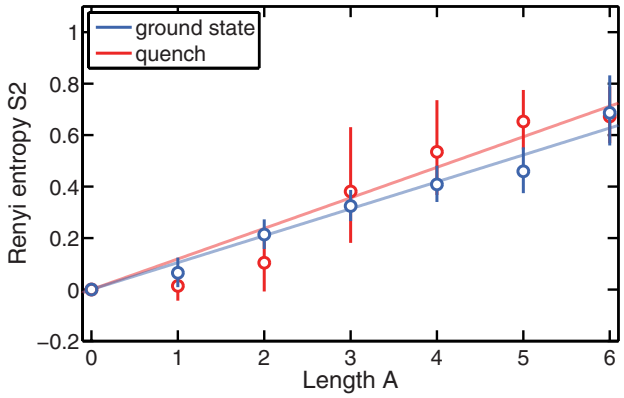

Figure S2: The difference between the measured Rényi entanglement entropy and theoretical calculation as a function of subsystem size. We use the entanglement entropy data of FIG. 4, averaged over contiguous and non-contiguous sub-systems; the subtracted theory exhibits the same averaging. The linear scaling indicates the presence of an extensive residual entropy background that we attribute to imperfections in the measurement protocol.

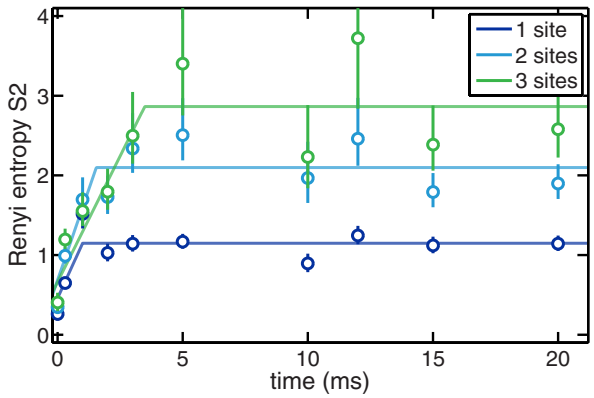

Figure S3: Piecewise linear fits to entanglement entropy dynamics for the three data sets of FIG. 3.

	V_x $[E_r]$	V_y $[E_r]$	$J_x/(2\pi)$ [Hz]	$U/(2\pi)$[Hz]	$T/(2\pi)$ [Hz]
initial state	45	45	0.07	172	0
quench I	6	45	66	103	249
quench II	2	45	178	68	1965

Table S1: Experimental parameters for the Hubbard chains. The initial Mott insulating state deep in the atomic limit $J_x \ll U$ is projected onto Bose-Hubbard chains with larger values of J_x/U, corresponding to different effective canonical temperatures T. All numerical simulations in the main text use the parameter values listed here.

	Theory	Data
Figure 2B	N/A	No Corrections
Figure 3	Offset Added	No Corrections
Figure 4	No Corrections	Extensive Entropy Subtracted

Table S2: Listing of all figures that contain data and the numerical corrections applied based upon residual extensive entropy in the system due to beam splitter infidelity.

References and Notes

1. J. J. Sakurai, *Modern Quantum Mechanics* (Addison Wesley Longman, 1993).

2. P. Calabrese, J. Cardy, Evolution of entanglement entropy in one-dimensional systems. *J. Stat. Mech.* **2005**, P04010 (2005). doi:10.1088/1742-5468/2005/04/P04010

3. L. Amico, R. Fazio, A. Osterloh, V. Vedral, Entanglement in many-body systems. *Rev. Mod. Phys.* **80**, 517–576 (2008). doi:10.1103/RevModPhys.80.517

4. A. J. Daley, H. Pichler, J. Schachenmayer, P. Zoller, Measuring entanglement growth in quench dynamics of bosons in an optical lattice. *Phys. Rev. Lett.* **109**, 020505 (2012). Medline doi:10.1103/PhysRevLett.109.020505

5. J. Schachenmayer, B. P. Lanyon, C. F. Roos, A. J. Daley, Entanglement growth in quench dynamics with variable range interactions. *Phys. Rev. X* **3**, 031015 (2013).

6. J. M. Deutsch, Quantum statistical mechanics in a closed system. *Phys. Rev. A* **43**, 2046–2049 (1991). Medline doi:10.1103/PhysRevA.43.2046

7. M. Rigol, V. Dunjko, M. Olshanii, Thermalization and its mechanism for generic isolated quantum systems. *Nature* **452**, 854–858 (2008). Medline doi:10.1038/nature06838

8. J. Eisert, M. Friesdorf, C. Gogolin, Quantum many-body systems out of equilibrium. *Nat. Phys.* **11**, 124–130 (2015). doi:10.1038/nphys3215

9. R. V. Jensen, R. Shankar, Statistical behavior in deterministic quantum systems with few degrees of freedom. *Phys. Rev. Lett.* **54**, 1879–1882 (1985). Medline doi:10.1103/PhysRevLett.54.1879

10. M. Srednicki, Chaos and quantum thermalization. *Phys. Rev. E* **50**, 888–901 (1994). Medline doi:10.1103/PhysRevE.50.888

11. L. F. Santos, A. Polkovnikov, M. Rigol, Weak and strong typicality in quantum systems. *Phys. Rev. E* **86**, 010102 (2012). Medline doi:10.1103/PhysRevE.86.010102

12. J. M. Deutsch, H. Li, A. Sharma, Microscopic origin of thermodynamic entropy in isolated systems. *Phys. Rev. E* **87**, 042135 (2013). Medline doi:10.1103/PhysRevE.87.042135

13. L. D'Alessio, Y. Kafri, A. Polkovnikov, M. Rigol, https://arxiv.org/abs/1509.06411v1 (2015).

14. C. Neill, P. Roushan, M. Fang, Y. Chen, M. Kolodrubetz, Z. Chen, A. Megrant, R. Barends, B. Campbell, B. Chiaro, A. Dunsworth, E. Jeffrey, J. Kelly, J. Mutus, P. J. J. O'Malley, C. Quintana, D. Sank, A. Vainsencher, J. Wenner, T. C. White, A. Polkovnikov, J. M. Martinis, https://arxiv.org/abs/1601.00600 (2016).

15. G. Clos, D. Porras, U. Warring, T. Schaetz, http://arxiv.org/abs/1509.07712 (2015).

16. S. Trotzky, Y.-A. Chen, A. Flesch, I. P. McCulloch, U. Schollwöck, J. Eisert, I. Bloch, Probing the relaxation towards equilibrium in an isolated strongly correlated one-dimensional Bose gas. *Nat. Phys.* **8**, 325–330 (2012). doi:10.1038/nphys2232

17. T. Langen, R. Geiger, M. Kuhnert, B. Rauer, J. Schmiedmayer, Local emergence of thermal correlations in an isolated quantum many-body system. *Nat. Phys.* **9**, 640–643 (2013). doi:10.1038/nphys2739

18. R. Geiger, T. Langen, I. E. Mazets, J. Schmiedmayer, Local relaxation and light-cone-like propagation of correlations in a trapped one-dimensional Bose gas. *New J. Phys.* **16**, 053034 (2014). doi:10.1088/1367-2630/16/5/053034

19. T. Langen, S. Erne, R. Geiger, B. Rauer, T. Schweigler, M. Kuhnert, W. Rohringer, I. E. Mazets, T. Gasenzer, J. Schmiedmayer, Experimental observation of a generalized Gibbs ensemble. *Science* **348**, 207–211 (2015). Medline doi:10.1126/science.1257026

20. R. Nandkishore, D. A. Huse, Many-body localization and thermalization in quantum statistical mechanics. *Annu. Rev. Condens. Matter Phys.* **6**, 15–38 (2015). doi:10.1146/annurev-conmatphys-031214-014726

21. W. S. Bakr, A. Peng, M. E. Tai, R. Ma, J. Simon, J. I. Gillen, S. Fölling, L. Pollet, M. Greiner, Probing the superfluid-to-Mott insulator transition at the single-atom level. *Science* **329**, 547–550 (2010). Medline

22. J. F. Sherson, C. Weitenberg, M. Endres, M. Cheneau, I. Bloch, S. Kuhr, Single-atom-resolved fluorescence imaging of an atomic Mott insulator. *Nature* **467**, 68–72 (2010). Medline doi:10.1038/nature09378

23. P. Zupancic, P. M. Preiss, R. Ma, A. Lukin, M. Eric Tai, M. Rispoli, R. Islam, M. Greiner, Ultra-precise holographic beam shaping for microscopic quantum control. *Opt. Express* **24**, 13881–13893 (2016). Medline doi:10.1364/OE.24.013881

24. Materials and methods are available as supplementary materials on *Science* Online.

25. R. Islam, R. Ma, P. M. Preiss, M. E. Tai, A. Lukin, M. Rispoli, M. Greiner, Measuring entanglement entropy in a quantum many-body system. *Nature* **528**, 77–83 (2015). Medline doi:10.1038/nature15750

26. C. A. Sackett, D. Kielpinski, B. E. King, C. Langer, V. Meyer, C. J. Myatt, M. Rowe, Q. A. Turchette, W. M. Itano, D. J. Wineland, C. Monroe, Experimental entanglement of four particles. *Nature* **404**, 256–259 (2000). Medline doi:10.1038/35005011

27. R. N. Palmer, C. Moura Alves, D. Jaksch, Detection and characterization of multipartite entanglement in optical lattices. *Phys. Rev. A* **72**, 042335 (2005). doi:10.1103/PhysRevA.72.042335

28. K. R. A. Hazzard, M. van den Worm, M. Foss-Feig, S. R. Manmana, E. G. Dalla Torre, T. Pfau, M. Kastner, A. M. Rey, Quantum correlations and entanglement in far-from-equilibrium spin systems. *Phys. Rev. A* **90**, 063622 (2014). doi:10.1103/PhysRevA.90.063622

29. R. Horodecki, P. Horodecki, M. Horodecki, K. Horodecki, Quantum entanglement. *Rev. Mod. Phys.* **81**, 865–942 (2009). doi:10.1103/RevModPhys.81.865

30. R. Horodecki, M. Horodecki, Information-theoretic aspects of inseparability of mixed states. *Phys. Rev. A* **54**, 1838–1843 (1996). Medline doi:10.1103/PhysRevA.54.1838

31. M. Cheneau, P. Barmettler, D. Poletti, M. Endres, P. Schauß, T. Fukuhara, C. Gross, I. Bloch, C. Kollath, S. Kuhr, Light-cone-like spreading of correlations in a quantum many-body system. *Nature* **481**, 484–487 (2012). Medline doi:10.1038/nature10748

32. P. Richerme, Z. X. Gong, A. Lee, C. Senko, J. Smith, M. Foss-Feig, S. Michalakis, A. V. Gorshkov, C. Monroe, Non-local propagation of correlations in quantum systems with long-range interactions. *Nature* **511**, 198–201 (2014). Medline doi:10.1038/nature13450

33. P. Calabrese, J. Cardy, Entanglement entropy and quantum field theory. *J. Stat. Mech.* **2004**, P06002 (2004).

34. J. Eisert, M. Cramer, M. B. Plenio, Colloquium: Area laws for the entanglement entropy. *Rev. Mod. Phys.* **82**, 277–306 (2010). doi:10.1103/RevModPhys.82.277

35. J. R. Garrison, T. Grover, https://arxiv.org/abs/1503.00729 (2015).

36. T. Grover, M. P. A. Fisher, Entanglement and the sign structure of quantum states. *Phys. Rev. A* **92**, 042308 (2015). doi:10.1103/PhysRevA.92.042308

37. M. M. Wolf, F. Verstraete, M. B. Hastings, J. I. Cirac, Area laws in quantum systems: Mutual information and correlations. *Phys. Rev. Lett.* **100**, 070502 (2008). Medline doi:10.1103/PhysRevLett.100.070502

38. D. N. Page, Average entropy of a subsystem. *Phys. Rev. Lett.* **71**, 1291–1294 (1993). Medline doi:10.1103/PhysRevLett.71.1291

39. K. Hyungwon, "Quantum nonequilibrium dynamics: Transport, entanglement, and thermalization," thesis, Princeton University (2014).

40. V. Yurovsky, A. Ben-Reuven, M. Olshanii, Dynamics of relaxation and fluctuations of the equilibrium state in an incompletely chaotic system. *J. Phys. Chem. B* **115**, 5340–5346 (2011). doi:10.1021/jp109388x

41. S. K. Ma, *Statistical Mechanics* (World Scientific, 1985).

42. K. Huang, *Statistical Mechanics* (John Wiley and Sons, 1963).

43. T. Kinoshita, T. Wenger, D. S. Weiss, A quantum Newton's cradle. *Nature* **440**, 900–903 (2006). Medline doi:10.1038/nature04693

44. M. Žnidarič, T. Prosen, P. Prelovšek, Many-body localization in the Heisenberg *XXZ* magnet in a random field. *Phys. Rev. B* **77**, 064426 (2008). doi:10.1103/PhysRevB.77.064426

45. J. H. Bardarson, F. Pollmann, J. E. Moore, Unbounded growth of entanglement in models of many-body localization. *Phys. Rev. Lett.* **109**, 017202 (2012). Medline doi:10.1103/PhysRevLett.109.017202

46. M. Serbyn, Z. Papić, D. A. Abanin, Universal slow growth of entanglement in interacting strongly disordered systems. *Phys. Rev. Lett.* **110**, 260601 (2013). Medline doi:10.1103/PhysRevLett.110.260601

47. M. Schreiber, S. S. Hodgman, P. Bordia, H. P. Lüschen, M. H. Fischer, R. Vosk, E. Altman, U. Schneider, I. Bloch, Observation of many-body localization of interacting fermions in a quasirandom optical lattice. *Science* **349**, 842–845 (2015). Medline